Effects of the anode material on the evolution of the vacuum breakdown process

Zhipeng Zhou[1,2], Andreas Kyritsakis[2], Zhenxing Wang[1*], Yi Li[1], Yingsan Geng[1], Flyura Djurabekova[2,3]

[1] *State Key Laboratory of Electrical Insulation and Power Equipment, Xi'an Jiaotong University, Xi'an 710049, China*

[2] *Helsinki Institute of Physics and Department of Physics, University of Helsinki, P.O. Box 43, FI-00014 Helsinki, Finland*

[3] *National Research Nuclear University MEPhI, Kashirskoye sh. 31, 115409 Moscow, Russia*

*zxwang@xjtu.edu.cn

Abstract

Vacuum breakdown, also known as vacuum discharge, is a common phenomenon in nature and gains an increasingly important role in modern technologies. In spite of a remarkable advance in understanding of the nature of the breakdown, the role of an anode, i.e. a positively charged electrode, in the development of the breakdown is still completely unclear. In this paper, we employ a streak camera with picosecond time resolution to observe precisely the evolution of anodic glow from different anode materials.

The results show that the choice of the anode material does not affect neither the delay time between the cathodic and anodic flares, nor the formation of the conductive channel. Furthermore, we show that the heating of the anode surface by runaway electron currents is not sufficient to evaporate enough atoms for the anodic glow. On the other hand, we show that the neutrals for the anodic flare can be produced by the ions from the expanding cathode plasma by sputtering.

Finally, the coincidence in time of the voltage collapse and the anode glow is consistent with the fast expansion of the cathode plasma, which causes both the voltage collapse and the anode glow when it reaches the anode and densifies by sputtering and reflection. However, the two events are not in direct dependence of one another, since the order of the appearance of them is random, implying that a fully conductive channel can be established without any light emission from the anode.

1. Introduction

Vacuum breakdowns occur under many circumstances, including fusion devices [1, 2], satellite systems [3, 4] and vacuum interrupters [5]. In particular, in high electric field applications like the Compact Linear Collider (CLIC) [6-8] and micro or nano electro-mechanical system (MEMS or NEMS) and capacitors [9, 10], breakdowns are the main performance limiting factors. For example, microfabricated devices such as the nano-electrospray thruster arrays for spacecraft may withstand large electric fields between electrodes, but if proper care is not taken arcs can occur, destroying the chip [11]. Also, the high accelerating field of 10^8 V/m in CLIC causes electrical breakdowns in the form of local vacuum arcs near surfaces of the accelerating

structures, resulting in beam destabilization, surface degradation and damage of the accelerating structures [7].

In general, the majority of both theoretical and experimental studies focus on tiny tips on the cathode in a vacuum gap, and it is usually proposed that a vacuum breakdown originates from these tips. For instance, Mesyats et al. [12, 13] have proposed the 'ECTON' model to explain the mechanism that can trigger a vacuum arc. In this model, the strong runaway currents are assumed to cause local surface explosion triggering formation of a vacuum arc. An alternative mechanism was proposed recently in [14]. The results of multiscale simulations revealed that a thermal runaway developed in Cu nanotips on the surface of a cathode is able to supply neutrals and electrons at the rates close to the threshold values defined in the independent Particle-In-Cell (PIC) simulations [15, 16]. However, from the perspective of experimental studies, it is important to note that a vacuum breakdown is triggered by strong local electric fields in the order of 10^{10} V/m [7]. These fields are able to cause deformation on the surface [17, 18], initiate intensive field emission currents [19], which heat the field-emitting tips through the Joule [20, 21] and Nottingham effects [22]. The intensive processes involving dynamics of energetic electrons at the cathode may result in light emission at this electrode [23-27]. The existence of this cathodic glow throughout the whole breakdown process shows its active role in initiating and maintaining vacuum arcs.

During the initial phase of a vacuum breakdown process, the cathodic glow is usually accompanied by an anodic glow [5, 25, 26], however, the nature of this anodic glow and the mechanisms leading to it are not yet been fully understood. Because the anodic glow may decay and even disappear in the stable burning phase of a diffuse vacuum arc, it is generally accepted that the anode is a passive absorber, which collects the electrons or other particles generated at the cathode [5, 28]. In the initial phase of a vacuum breakdown, however, the experimental results [23-27] show an interesting behavior of anodic glow: the illumination that appears initially near the anode surface expands rapidly during the breakdown process towards the cathode. Furthermore, the volume of the anodic glow is much larger than that of the cathodic one and the size of the craters left on the anode surface might also be larger than of those found on the cathode [29]. Based on these observations, some researchers conclude that the anode plays a decisive role in the initial stage of a vacuum breakdown [30, 31]. Especially when the light emission in breakdowns was investigated in relation to the formation of a conductive channel in vacuum gaps, the appearance and expansion of the anodic glow were considered to be prerequisites for the establishment of the conductive path, because the gap voltage was observed to collapse only when the expanding anodic glow meets the cathodic one [25, 27, 32, 33].

We also did similar investigations in our previous work, where we observed the evolution of vacuum breakdowns by using an ICCD (Intensified Charge-Coupled Device) camera with nanosecond resolution [26] and recorded the voltage and current waveforms at the meantime. By analyzing the light emission photos and current-voltage curves, however, we found that the expansion of the anodic glow is not necessary for the formation of the conductive channel in vacuum gaps, because the gap voltage can collapse well before the anodic glow meets the

cathodic one. We also concluded that the anodic glow is a secondary phenomenon originating due to the particles directing from the cathode to the anode, but the detailed processes that produce the anodic glow are still unknown. On the other hand, investigating the nature and formation mechanism of the anodic glow can help deepen the understanding for the cathode plasma expansion and the establishment of the conductive channel in vacuum breakdowns. Therefore, the objective of this paper is to investigate experimentally the prerequisites for the appearance of the anodic glow and its role in the vacuum breakdown evolution. To improve the precision of the obtained results, we used a streak camera with high-time resolution up to several pico-seconds. We performed a comparative study of the six different anode materials, three different gap lengths and two values of steady currents. We discuss the obtained results with respect to the processes that ignite the anodic glow.

2. Experiments

2.1. General description

Figure 1 shows the experimental setup. A demountable stainless-steel chamber was used to conduct breakdown experiments, with its pressure pumped down to 2.5×10^{-4} Pa by a turbo molecular pump. Breakdowns happened between a pair of electrodes installed in the vacuum chamber, and the gap length can be adjusted by a micrometer manipulator. The high voltage was supplied to the upper electrode, while the lower electrode was grounded. The voltage provided by the impulse source ranges from 0 to -50 kV with a pulse width between 1 and 5 μs. The light emission during the breakdowns was observed by a streak camera through one of the glass windows of the vacuum chamber.

The streak camera is manufactured by the Xi'an Institute of Optics and Precision Mechanics of Chinese Academy of Sciences (XIOPM). The structure and working principle of the camera is shown in Figure 2. It can resolve a one-dimensional object with a high time resolution up to several pico-seconds. It consists of a slit, a photocathode, a scanning circuit, a deflector, a microchannel plate (MCP), a fluorescent screen and a CCD (Charge-Coupled Device) camera. The slit is used to select the area (a narrow area of tens of micrometers, i.e. the one-dimensional object) to be observed, and its width can be adjusted. The object to be observed is imaged at the slit position via a lens, and the photocathode is irradiated by the light passing through the slit to generate photoelectrons. These photoelectrons are then accelerated by a high voltage extraction grid toward the MCP and the screen. Before the electrons arrive at the MCP, they are deflected by the deflection voltage, provided by the scanning circuit. The magnitude of the latter changes over time so that electrons entering the deflector at different times have different displacements and eventually reach different positions on the screen. The direction of the deflection electric field and the direction of the slit are perpendicular to each other. Therefore, in an image captured by the streak camera, the vertical direction corresponds to a narrow (or one-dimensional) area of the object to be observed, while the horizontal direction represents the time evolution of the light intensity in the observed narrow area. The function of the MCP is to increase the number of electrons and enhance the weak light signal of the observed object, thereby improving the sensitivity of the streak camera. The detectable wavelength of the streak camera ranges from 200 – 850 nm, and its spatial resolution is better than 20 μm.

The streak camera was mounted on a 3D movable optical table and equipped with an adjustable zoom lens, which makes it easier to obtain clear images of the discharges. The voltage across the gap and the current were measured by a high voltage probe (NorthStar PVM-7, 100 kV and 110 MHz) and a Pearson current sensor (Model 6595, 200 MHz) respectively, and recorded by a four-channel oscilloscope with a sample rate of 500 MHz. Finally, a digital delay generator (SRS DG645) acted as a master control to trigger the impulse voltage source, the streak camera and the oscilloscope with a proper timing sequence.

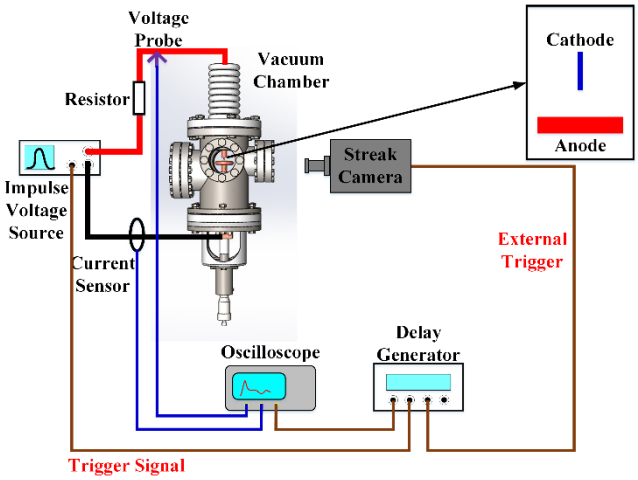

Figure 1. Schematic diagram of the experimental setup.

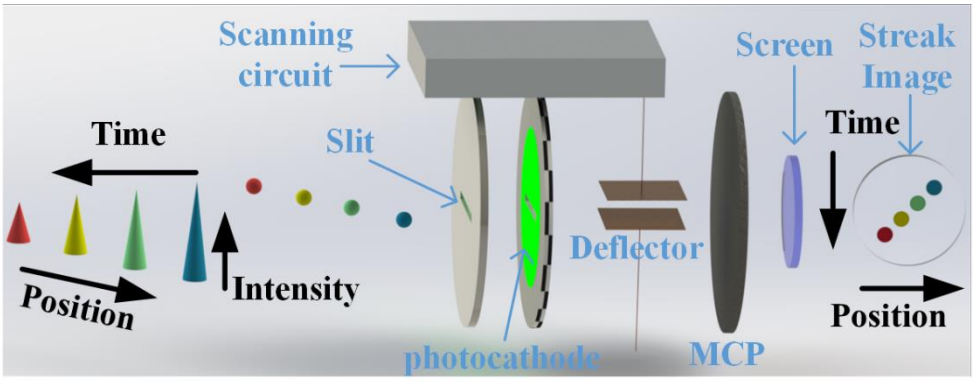

Figure 2. Structure and working principle for a streak camera.

2.2. Electrode configuration

A tip-to-plane electrode configuration as shown in Figure 1 was used. The tip electrode is a wire with a conical tip, whose diameter and tip angle (full apex angle) are respectively 1 mm and 15°, while the plane electrode is a cylinder with a diameter of 40 mm and a thickness of 10 mm. Since the voltage source supplied high voltages with negative values, the upper (tip) electrode connected to the high voltage terminal of the voltage source was the cathode in the configuration. The anode material varied among Al, Cr, Cu, Mo, Ni and W, while the cathode material was always Cu. The relevant physical properties of these materials are summarized in Table 1 for the reference in the following sections. For each anode material, we used a fresh cathode tip. The gap lengths were 2.5 mm, 5 mm and 10 mm.

Table 1. Physical properties of anode materials in the experiments.

	Al	Cr	Cu	Mo	Ni	W
Melting point (K)	933	2133	1356	2890	1728	3643
Boiling point (K)	2792	2944	2835	4912	3186	6173
Vaporization heat (J/g)	9462	5945	5234	5610	5862	4477

2.3. Experimental procedure

First, a desired maximum voltage was set on the voltage source to be sufficiently high to trigger a vacuum breakdown at every pulse. The steady-state arc current is determined by this maximum applied voltage and a current-limiting resistor of 500 Ω. We shall refer to this voltage as "pulse voltage", although the potential difference between the electrodes never reaches this value because of the occurrence of breakdowns. We used -30 kV and -40 kV to generate arc currents of 60 A and 80 A respectively. The pulse width in this paper was set uniformly to 5 μs, with the actual output time a little longer. This small difference in pulse width has no impact on the discussions and conclusions in the paper, since we only focused on the initial stage of a breakdown process.

Then the optical table and lens were adjusted to get a clear view of the electrodes as shown in Figure 3. The tip cathode is on the top, while the plane anode is at the bottom, with its surface outlined by a dash line. The tip cathode was located at the center of the slit of the streak camera, which was shrunk to 30 μm before a capture began.

Finally, a proper scanning time, i.e. the time corresponding to the total width of a streak camera image as shown in Figure 5, was chosen according to the time scale of the observed process. This camera has five different scanning times to be chosen from, which are 1 ns, 10 ns, 100 ns, 1 μs and 10 μs.

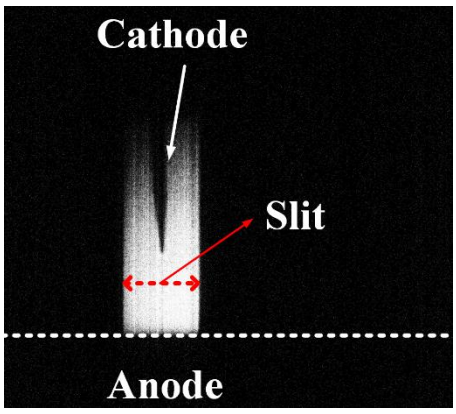

Figure 3. Sample image of the electrodes and gap.

3. Results

In order to obtain feasible and accurate data, we repeated 30 experiments for each condition, including different anode materials (Al, Cr, Cu, Mo, Ni and W), different gap lengths (2.5 mm,

5 mm and 10 mm), and different pulse voltages (30 and 40 kV). All the possible combinations of anode material, gap length and pulse voltage were tested in this work. In order to eliminate variations caused by the cathode material, a copper cathode was selected for all cases.

3.1. The typical electrical waveforms and corresponding streak images

Figure 4 shows the typical voltage and current waveforms of a vacuum breakdown process. The gap length was 5 mm, and the pulse voltage was 40 kV. Figure 4(a) is for the waveforms of the entire process, while Figure 4(b) is an enlarged view of the initial stage of the curves. The voltage and current are marked by different colors, blue and red, respectively. In Figure 4(b), we can see that the current starts to rise dramatically from the point t_{BD}, indicating the initiation of a breakdown process. The small current before t_{BD} corresponds to the charging of the gap, and t_{BD} is defined at the inflexion point (zero second order gradient) of current as shown in Figure 4(b). For the convenience of description, the starting point of breakdown, t_{BD}, is defined as the time zero in the measurements.

As the current rises, the voltage between the gaps gradually decreases and eventually reaches zero at time t_{FB}, which indicates the establishment of a conductive channel and a full breakdown of the vacuum gap. Afterwards, both the voltage and the current transit into steady values, and the breakdown process enters the vacuum arc stage. The steady values were determined and restricted by the external circuit. The gap remained in a high-current and low-voltage state until the external impulse voltage source was turned off at time t_E, after which the current drops rapidly to zero. The turn-on duration for the voltage source was about 5 μs, which can be verified by the current pulse width in Figure 4.

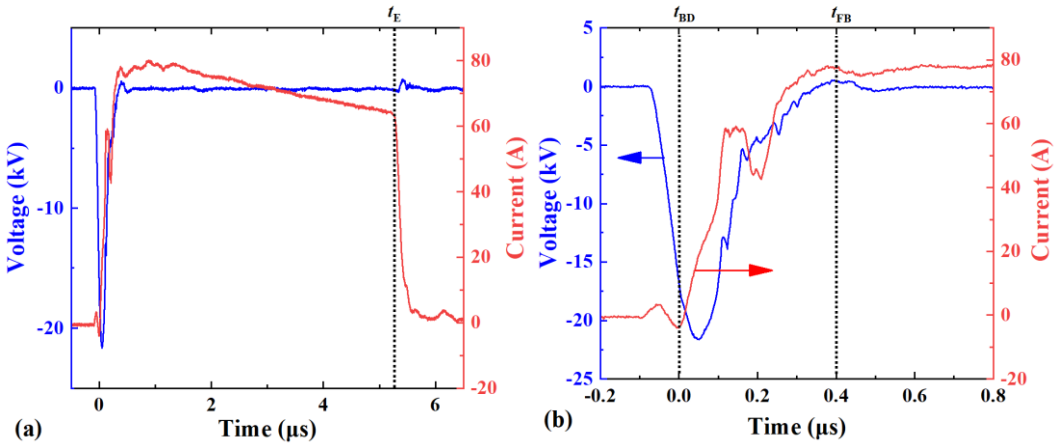

Figure 4. Typical voltage and current waveforms of a vacuum breakdown process. The voltage is shown as the blue and the current as the red curves. (a) The waveforms of the entire process; (b) an enlarged graph of the initial stage. Gap length: 5 mm; pulse width: 5 μs; pulse voltage: 40 kV. t_{BD}: starting point of a breakdown; t_{FB}: the time point for a transition to a steady state; t_E: the time point of voltage source turn-off.

Figure 5 shows the corresponding streak image for the same discharge as shown in Figure 4. The horizontal axis of this image represents time lapsing, from left to right, rather than positions in space. The total observing duration corresponding to the full width of the image (TDFW)

was 10 μs. The zero point of the time axis is the starting point of the breakdown process, t_{BD}, as defined in Figure 4. The vertical axis represents the spatial position, with zero point being the position of the cathode tip and the -5 mm for the position of the anode surface. A schematic for the electrodes and two dashed lines were also attached on the image to indicate the positions of the cathode and the anode. As shown in Figure 5, the cathode started glowing at time t_{CG}, which almost coincides with t_{BD} in Figure 4. This means that the cathodic glow starts immediately after a vacuum breakdown was triggered. After about 300 ns, anodic glow can be observed at time t_{AG}, with the glowing region expanding towards the cathode with a steady speed of about 4000 m/s, given by the slope of the glow expansion line (the purple dotted line) in Figure 5. The intensity of the anodic glow does not appear to increase, but on contrary, it starts decaying after a short time, while the cathodic glow becomes stronger until the discharge was turned off after t_E, when the voltage pulse ceased providing energy. We can see in Figure 5 that the existence duration of the cathodic glow is also about 5 μs, which is consistent with the duration of the voltage pulse.

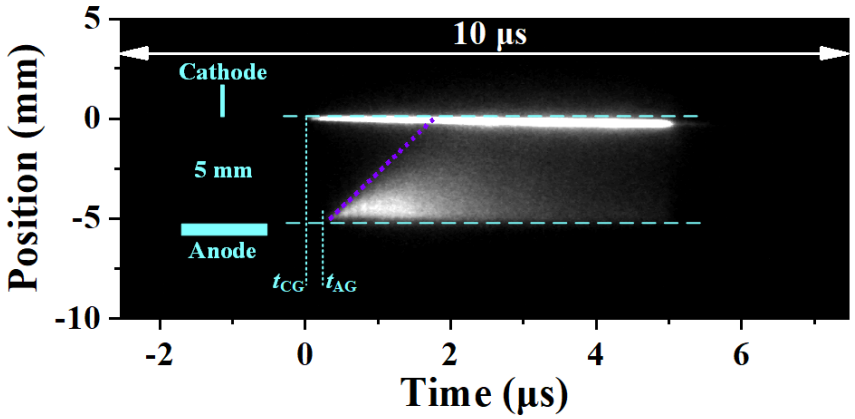

Figure 5. A streak image for a vacuum breakdown process. TDFW: 10 μs; gap length: 5 mm; pulse width: 5 μs; pulse voltage: 40 kV; anode material: Cu. t_{CG}: the starting point of cathodic glow, t_{CG}=t_{BD}; t_{AG}: starting point of anodic glow. The delay time between cathodic and anodic glow, t_{AG}-t_{CG}, was measured to be about 300 ns. The purple dotted line indicates the expansion of the anodic glow.

3.2. The effect of anode materials on the anodic glow delay

As shown in Figure 5, the tip of the cathode started glowing immediately after a vacuum breakdown occurred, while there was a time delay between the cathodic and anodic glow. In our previous paper, we found that this time lag ranged from tens of nanoseconds to hundreds of nanoseconds depending on gap lengths. In this paper, we investigate the effect of anode materials on the delay time.

Figure 6 shows the current waveforms under different experimental conditions. We compared two gap lengths (2.5 mm and 10 mm), two pulse voltages (30 and 40 kV), and all the anode materials (Al, Cr, Cu, Mo, Ni and W). The behaviors of the current waveforms were significantly affected by the gap length and the pulse voltage. Shorter gap lengths correspond to significantly faster current rising. However, after the rising stage, the current stabilizes to a value determined by the external resistor and the pulse voltage, regardless of the gap length.

On the other hand, the anode material does not have any significant influence on the behavior of the current. For instance, we observe almost identical current curves through the gap of the same size and at the same voltage for all different anode materials. Considering the significant differences between the material properties, this implies that the anode material plays only a marginal role in the transition to the steady state vacuum arc in a breakdown process.

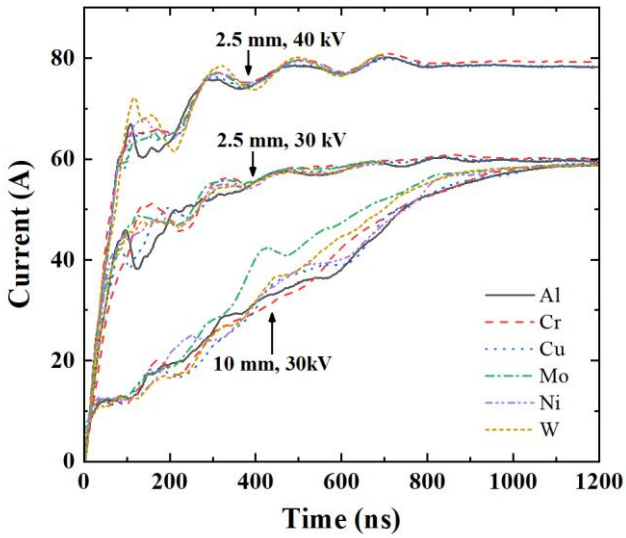

Figure 6. Current waveforms for the initial stage of vacuum breakdowns.

In the image shown in Figure 7, we adjusted the TDFW parameter of the streak camera to 1μs in order to focus on the initial stage of a breakdown. The zero point of the time axis is the starting point of the breakdown process, t_{BD}, as defined in Figure 4. The vertical axis represents the spatial position, with zero point being the position of the cathode tip and the anode plane being at -5 mm. The anode material was copper; the pulse voltage was 40 kV. As shown in Figure 7, the delay time between cathodic and anodic glow, t_{AG}-t_{CG}, was measured to be about 331 ns. Using similar streak camera shots, we obtained the delay times for all combinations of experimental conditions.

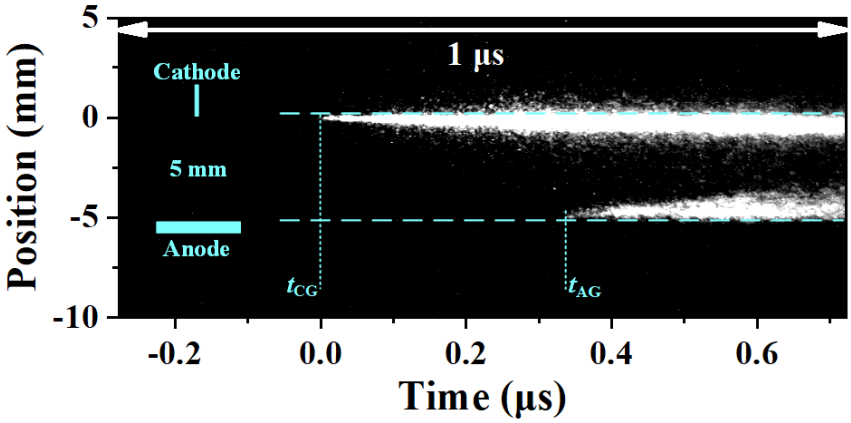

Figure 7. A streak image for the initial stage of a vacuum breakdown. TDFW: 1 μs; gap length: 5 mm; voltage pulse width: 5 μs; pulse voltage: 40 kV; anode material: Cu. The delay time between cathodic and anodic glow, t_{AG}-t_{CG}, was measured to be about 331 ns.

Figure 8 shows comprehensively the delay times of the anodic glow from the start of the cathodic one obtained for different anode materials under different experimental conditions. The delays were obtained from streak images similar to Figure 7. In this figure, the results for the 2.5 mm gap length are shown in squares, for 5 mm in circles and for 10 mm in triangles. The closed symbols we used for the 30 kV pulse voltage, while the open ones show the results obtained with 40 kV voltage. The anode materials are Al, W, Cr, Cu, Mo, and Ni. The delay for each condition was averaged over 30 repetitions, with the standard deviation indicated by the error bars. In Figure 8 we observe that the increase of the arc current (increase of the pulse voltage) reduced the delay time notably. However, we observed stronger effect while increasing the gap length: the short delay times for the shortest gap length increase super linearly with increase of the gap length.

The unexpected feature in this graph, however, is found with respect to the choice of the anode material. Varying materials with significantly different properties did not result in any significant effect on the delay of the anodic glow. Indeed, the estimated standard deviations from the mean delay times obtained in the experiments with the same experimental conditions, but varying anode material, was found to range from 3% to 12% for different conditions. Surprisingly, within the experiments with the same material and the same experimental conditions (30 shots) the standard deviation ranged between 11% and 12%. Even in the case of Mo, the delay time, which appears to deviate the most from the rest of the materials, remains within the uncertainties observed for all materials.

This observation does not support the hypothesis that the anodic flare is formed by neutral atoms thermally evaporated from the anode surface heated by strong arc currents as it was suggested in number of publications, including our previous work [5, 25, 26, 32, 33]. Since the materials used in this series of experiments had very different thermal and mechanical properties, some correlation with the change of the anode material must have been observed if the anodic glow results from thermal evaporation of the anode surface.

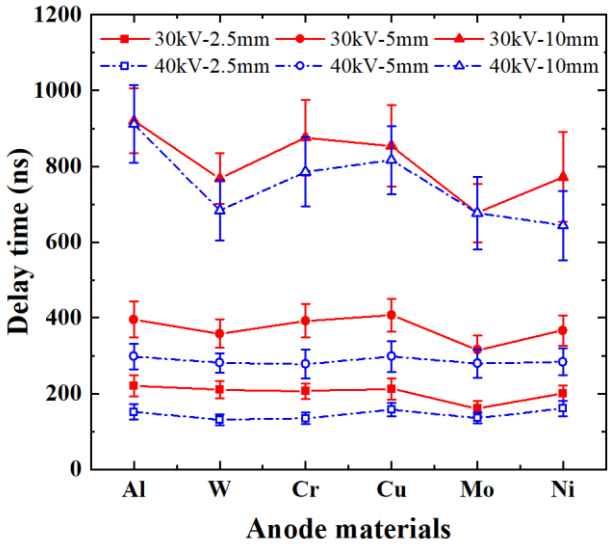

Figure 8. Comprehensive view of the delay times of the anodic glow appearance. Delay is measured from the moment when the illumination near the cathode was registered. The measurements are performed for different anode materials with two values of the pulse voltage (30 kV and 40 kV) applied to the electrodes

with the gaps of three different lengths (2.5mm, 5mm and 10mm). The delay for each condition was averaged over 30 repetitions, with the standard deviation indicated by the error bars.

In order to estimate the expected evaporation from the anode surface, we solved the heat diffusion equation in the anode. The energy carried by the incoming electrons is considered to deposit into a volume in the anode. The depth of the heated volume was estimated by the penetration depth of electrons (z_d) according to the "continuous slowing down approximation –CSDA", which can be found in the ESTAR database [34]. The area of the heated volume was determined by the beam size of the electrons, which can be estimated by the glowing area of on the anode surface. Since the depth of the heat deposition volume (several microns) is much smaller than its lateral dimensions (several millimeters), we ignored the lateral heat flow and solved the heat equation in one dimension in order to obtain the heat distribution and evolution. The heat equation can be written as

$$C_v \frac{\partial T}{\partial t} = \frac{\partial T}{\partial z}\left[\kappa(T)\frac{\partial T}{\partial z}\right] + p(z)$$

where C_v is the volumetric heat capacity, T is the temperature, t is the time, z is the depth, $\kappa(T)$ is the heat conductivity and $p(z)$ is the deposited heat density as a function of the material depth z.

We consider the deposited heating power density to be constant over the CSDA range, z_d, and zero deeper than it, i.e. $p(z > z_d) = 0$ and $p(z < z_d) = P/z_d$, with P being the deposited heating power per unit area. When estimating the power P, we assumed a Gaussian distribution for the electron beam at the anode surface with the distribution radius (σ) being 1 mm for a 5 mm gap, in line with our previous work [26]. Then the maximum incident power on the anode due to incoming electrons is $P(t)=V(t)I(t)/(2\pi\sigma^2)$, with $V(t)$ and $I(t)$ being the gap voltage and gap current, respectively.

The length of the calculation domain is 50 μm, with one end being the anode surface and the other end considered adiabatic. The adiabatic boundary condition can always be fulfilled during the calculation duration of 700 ns according to the temperature distribution in the results. The heat flux taken away by evaporation at the anode surface was considered by

$$q_{ev} = \frac{L_{ev}}{N_A}\phi$$

where L_{ev} is the heat of vaporization, N_A is the Avogadro's constant and ϕ is the rate of evaporation, which is calculated as follows,

$$\phi = \frac{p_{sat}}{\sqrt{2\pi kmT}}$$

where k is the Boltzmann constant, m is the atom mass and p_{sat} is the saturated vapor pressure calculated by the Clausius-Clapeyron equation as follows,

$$p_{sat} = p_{atm}\exp\left[-\frac{L_{ev}}{R}\left(\frac{1}{T}-\frac{1}{T_b}\right)\right]$$

where p_{atm} is the atmospheric pressure, R is the ideal gas constant and T_b is the boiling point of the material.

Taking the maximum incident power as a heat source for the anode and initial temperature of 300 K, we solve the heat diffusion equation and obtain the maximum temperature of the anode surface, which is plotted as a function of time in Figure 9(a). Then the corresponding number

density of the evaporated atoms (n^{ev}) near the anode surface was calculated according to the saturated vapor pressure and the gas state equation as follows

$$p_{sat}=n^{ev}kT$$

and is plotted in Figure 9(b).

The curves in Figure 9 were obtained by averaging over 30 shots of breakdown for each anode material, and the evolution starts from the breakdown instant. We performed the calculation for discharges with 40 kV pulse voltage and 5 mm gap. We can see that both anode temperature and evaporated atom density rose to their peak values at 200-300 ns, after that both values started decreasing rapidly. In these graphs, we observe strong correlation with the material, e.g. the temperature at the Cu anode is able to reach the lowest value, while the lowest vapor density (1×10^{12} m^{-3}) was still observed for tungsten, which is even lower than the vacuum maintained in the gap (about 6×10^{16} m^{-3} at 300 K). These results clearly indicate that it is not possible for W and Mo anodes to light up under the assumption that the atoms for the glow near the anode are provided by the evaporation process. Moreover, Cr has a quite high vapor density of about 1×10^{23} m^{-3}, which is more than 11 orders of magnitude higher than that of W. This great difference in evaporated atom densities for different anode materials would also result in great difference in the delay for the anodic glow, if all the atoms in the anodic glow region come from the evaporation of the anode surface. Yet, we observed the existence of light emission near the anode for all anode materials with the corresponding time delays varying only marginally for different materials. Therefore, the anodic glow cannot be explained by thermal evaporation due to electron bombardment of the anode and alternative mechanisms have to be investigated.

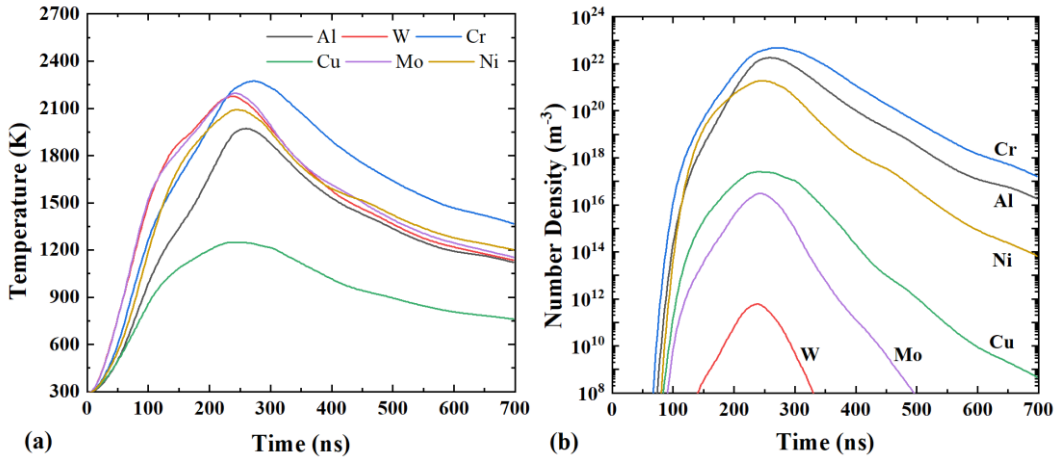

Figure 9. Calculation of the maximum temperature of the anode surface and the evaporated atom densities near the anode surface. The results were obtained by averaging over 30 times of breakdowns for each material. Gap length: 5 mm; pulse width: 5 μs; pulse voltage: 40 kV.

In our previous work performing spectroscopic observation on the anodic glow [35], we found that both the cathode and anode materials contribute significantly in the anodic glow. This implies that the cathodic flare must reach the anode so that the atoms of the cathode material can be identified near the anode. It has been suggested earlier [36, 37] that the anode flare ignites when the expanding cathode plasma reaches the anode and causes the sputtering of atoms from the anodic surface. To verify this hypothesis, we estimate the cathode plasma

expansion velocity to be about 20000 m/s according to the delay times of anodic glow and the corresponding gap lengths, as shown in Figure 8. This high value of the ion velocity was also found in a number of experimental and theoretical studies [36, 38-42]. Such a high ion velocity corresponds to sufficiently high kinetic energy to cause the sputtering of the neutral atoms from the anode surface. We calculated the sputtering yields and the average energy of a sputtered atom per incoming ion using the binary collision approximation code SRIM [43]. The incident energy of copper ions was set to 132 eV in all simulations, which corresponds to the velocity of 20000 m/s. The sputtering yields and velocity distribution of sputtered atoms were obtained and shown in Table 2.

Table 2. Sputtering yields (Y), average energy of a sputtered atom ($\langle E \rangle_{sp}$) and the average velocity of a sputtered atom ($\langle v \rangle_{sp}$) for all studied anode materials.

Anode materials	Al	W	Cr	Cu	Mo	Ni
Y	0.12	0.44	0.21	0.62	0.4	0.35
$\langle E \rangle_{sp}$ (eV/atom)	4	22.9	6.5	7.7	21.4	7.4
$\langle v \rangle_{sp}$ (m/s)	5349	4904	4912	4836	6562	4933

According to the estimations reported in Refs. [44, 45], the total current in the gap during a steady-state vacuum arc consists of up to 8% - 12% of the ion flux from the cathode to the anode. We see that in our experiments the vacuum discharge almost entered a steady state when the ions from the cathode reached the anode, so we assumed an ion flux corresponding to a current of I_{ion}=8 A (10% of the arc current) reaching the anode surface, in order to estimate the flux of the sputtered atoms. The distribution of the ion beam is assumed to be the same as the one estimated by analyzing the anode glow images in ref. [26], i.e. a Gaussian distribution with σ=1 mm. Thus the maximum ion flux density at the anode surface can be estimated as follows, assuming that all ions are single-charged:

$$Q=\frac{I_{ion}}{e}\frac{1}{2\pi\sigma^2}=7.96\times10^{24}\ \mathrm{m^{-2}\cdot s^{-1}}.$$

In the above equation, Q is the maximum ion flux density, e is the elementary charge and σ is the distribution radius of the ion beam, σ=1 mm. Then the sputtered atom density is estimated by

$$n^{sp}=\frac{QY}{v_{sput}}$$

where Y and v_{sput} are the sputtering yield and the average velocity of sputtered atoms in Table 2.

To produce the light of measurable intensity, e.g. seen in Figure 7, the atom densities near the anode must be sufficiently high. Moreover, the time required to build up the sufficient atom density will contribute to the delay of anodic glow. Hence, we compare the atom densities estimated from both assumptions, produced by sputtering and evaporation mechanisms. The sputtered atom densities estimated by this method are compared with evaporated atom densities of Figure 9(b) in the first two rows of Table 3. We can see that the evaporated atom density has higher values when the anode materials are Al, Cr and Ni, while the sputtered atom density has higher values for W, Cu and Mo anodes. However, the estimated sputtered atom densities are about 10^{20} $\mathrm{m^{-3}}$, not varying significantly for different materials. These results are consistent

with the experimental data of Figure 8. Therefore, we conclude that the sputtering of the anode surface under the impact of the expanding cathode plasma ions is an important source of atoms escaping from the anode, which contribute significantly on the ignition of the anode flare. This contribution has also been confirmed by our previous spectroscopic experiments [35].

Table 3. Comparison of the atomic densities produced by the sputtered (n^{sp}) and evaporated atoms (n^{ev}) for different anode materials. Gap length is 5 mm; applied voltage is 40 kV. Gaussian distribution for electron and ions within the beam radius is assumed.

Anode	Al	W	Cr	Cu	Mo	Ni
$n^{sp}_{\sigma=1mm}(m^{-3})$	1.79×10^{20}	7.14×10^{20}	3.40×10^{20}	1.02×10^{21}	4.85×10^{20}	5.65×10^{20}
$n^{ev}_{\sigma=1mm}(m^{-3})$	1.82×10^{22}	6.03×10^{11}	4.83×10^{22}	2.58×10^{17}	3.17×10^{16}	1.91×10^{21}
$n^{sp}_{\sigma=2mm}(m^{-3})$	4.46×10^{19}	1.79×10^{20}	8.51×10^{19}	2.55×10^{20}	1.21×10^{20}	1.41×10^{20}
$n^{ev}_{\sigma=2mm}(m^{-3})$	7.82×10^{4}	3.90×10^{-30}	2.15×10^{6}	9.62×10^{-3}	2.41×10^{-14}	3.81×10^{3}

Note that the radius σ of the irradiated spot was deduced from the snapshot of the initial stage of the anodic glow, see Ref. [26]. As one can see, this estimation of σ is not very accurate, while its value effects the calculation of the estimated atom density dramatically. Thus we need to analyze the uncertainty of our estimation. In Figure 9(a), we can see that the peak temperature for the copper anode reached 1200 K, which is close to the melting point of copper (1356 K). If we reduce the radius further, the estimated power density at the surface will increase, resulting in further increase of the temperature at the spot, that most likely would lead to its melting. Since we have not observed melting of the anode surface with 5 mm gap length [26], the assumed beam radius cannot be much smaller than 1 mm. In order to estimate the uncertainty of this calculation, we considered a larger spot radius of 2 mm. The corresponding results for σ=2 mm are shown in the last two rows of Table 3. The densities of sputtered atoms only decrease 4 times, while the densities of the evaporated atoms decline dramatically by more than ten orders of magnitude. This analysis supports further the hypothesis that the major contribution to the anodic glow comes from atoms sputtered from the anode surface due to impact of ions from the cathode.

3.3. The relation between the anodic glow and the voltage collapse

The current and voltage waveforms recorded during a vacuum breakdown, see Figure 4, describe the transient process from an insulating vacuum gap to a fully conductive channel between the electrodes. These processes exhibit themselves through the rapid current rise to a steady-state value and the voltage drops to almost zero. The full voltage collapse indicates the formation of the conductive channel in the gap. It is often considered that the bridging of the expanding anodic and the localized cathodic glows is prerequisite for formation of a conductive channel that causes the voltage collapse [5, 25, 32, 33], which we showed in Ref. [26] to be inconsistent with the time-resolved measurements of the evolution of the anodic glow and the voltage collapse (t_{FB}, see Figure 4). In this section, we discuss the correlation between the appearance of the anodic glow and the voltage collapse.

Figure 10 shows the comparison of delay times for the anodic glow appearance (t_{AG}-t_{CG}) and for the voltage collapse (t_{FB}-t_{BD}) under different conditions. Since the initiation of a vacuum

breakdown (t_{BD}) and the cathodic glow (t_{CG}) practically coincide, these two delays indicate the chronological order of the anodic glow a and the voltage collapse. Figure 10(a) is for 30 kV of the pulse voltage while Figure 10(b) for 40 kV. The open symbols and dashed lines in the figures represent the delay times for the anodic glow, while solid symbols and solid lines represent the delays for the voltage collapse. The delay times in the figure were obtained by averaging over 30 breakdown shots for each combination of the experimental conditions. As shown in the figures, the delay times for anodic glow and the voltage collapse are generally very close to each other. The difference between the average values is within the error bars indicating the standard deviation of the experimental measurements. Comparing all results, we note that the anodic glow tends to appear before the voltage collapse at higher applied voltages and shorter gaps (see the delay times obtained for 2.5 mm and 5 mm under 40 kV in Figure 10(b) for reference).

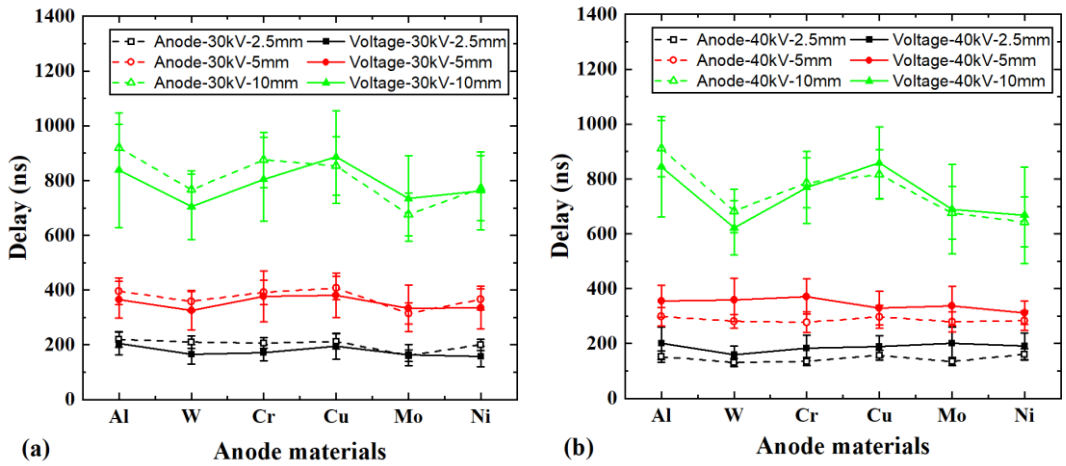

Figure 10. Comparison of delays for the anodic glow appearance and the voltage collapse under different conditions. (a) is for the 30 kV applied voltage and 60 A steady current cases, and (b) is for the 40 kV applied voltage and 80 A steady current case. Open symbols and dash lines represent the delays for the anodic glow, while solid symbols and solid lines represent the delays for the voltage collapse.

Furthermore, in Figure 11 we present the correlation between the two delay times of the anodic glow and of the voltage collapse for all breakdown shots performed in these experiments. The plot shows that there is a strong correlation between these two quantities. The high Pearson's correlation coefficient (ρ=0.94) and a slope of a fitted line, which is close to 1 (α=0.94) indicate that the two events are strongly correlated. This correlation indicates that the processes of the complete voltage drop and the ignition of the anodic glow are related, however, they are not in direct dependence of one another, since the order of the appearance of the two processes is random.

We note that both the voltage drop and the appearance of the anodic glow are consequences of the same process, namely the expansion of the cathodic plasma. As it was shown in section 3.2, the cathodic plasma ions arrive at the surface of the anode with rather high kinetic energies. The energies are sufficient to cause the sputtering and/or evaporation of slow atoms, which are able to interact with electrons giving rise to the anodic glow. However, it is not necessary that the full voltage drop takes place always before (or after) the anodic glow appears. Due to the stochastic nature of the processes at the cathode, the density of the expanding plasma may vary.

As a consequence, the sputtering caused by the cathodic plasma ions may be stronger (or weaker) when the full conducting channel was established in the gap.

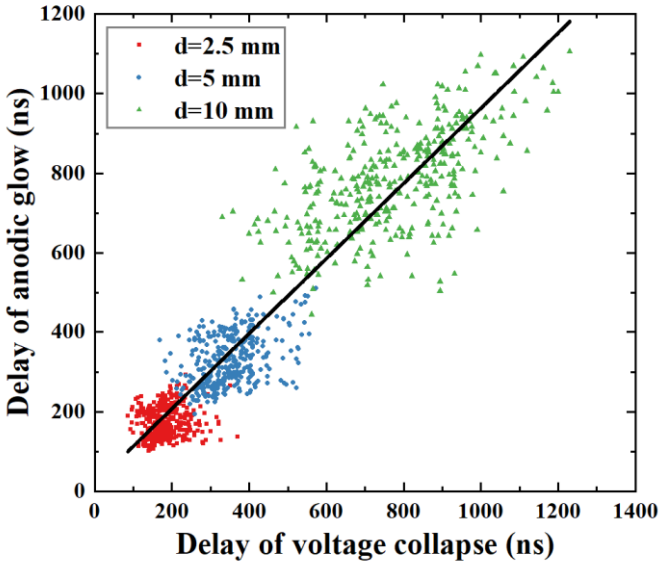

Figure 11. Comparison of delay times for the appearance of the anodic glow and the voltage collapse in all experiments. The straight line is a linear fit with a slope α=0.944 and intercept 17 ns. The Pearson correlation coefficient is ρ=0.938.

4. Discussion

The present experiments confirm that the vacuum breakdown initiates from the cathode. Although this observation is not debated any more, the dynamic evolution of the plasma within the gap is still not completely clear. In the images taken by the streak camera (see Figure 5) and by ICCD cameras (see ref. [26]), the cathode plasma seems to remain in the vicinity of the cathode, while the anode glow seems to be disconnected from it. This observation motivated the explanation of appearance of the anodic glow as a result of material evaporation from the anode surface heated by energetic electrons, as proposed in [26] as well as in many other references [5, 25, 32, 33].

In this scenario, the electrons escaping from the anode-facing plasma boundary are accelerated by the high voltage between the anode and the plasma. This voltage remains across the gap during the initial breakdown stage. The escaped electrons acquire high energies and heat the anode surface upon arrival. Hence, it is plausible to assume that these electrons induce the emission of neutral atoms through efficient local heating at the anode surface. While not excluding this mechanism, the results of the current experiments show that electronic heating cannot be a major source of vapor atoms for the following reasons:

1) The densities of the evaporated atoms vary by several orders of magnitude among different anode materials, while the dynamics of the anodic glow appear to be very similar (see Figure 8 and Figure 9).
2) The evaporated atom densities for some anode materials are not sufficient to emit light, while we observed light emission at anodic region for all the materials (see Figure 9).

3) The estimated vapor densities are extremely sensitive to the estimation of the radius of the electron beam, which can only be larger than the value we used in the current estimations. Hence, the densities of evaporated atoms can only decrease, if more accurate assessment of the electronic heating were possible.

However, if the current is high enough or the electron beam radius is small enough (in short gaps for example), electron heating on the anode may also contribute largely to the anode glow, but this is beyond the scope of this paper.

On the other hand, the plasma expansion scenario proposed by Anders[36, 37] is consistent with the present experimental results. According to this, the cathode plasma gradually expands from the cathode, although it glows only in its vicinity. During this expansion, the quasi-neutral plasma occupies an increasing fraction of the gap volume, while the gap voltage decreases gradually as shown in Figure 4 and other simulation works [40, 41, 46]. The rate of plasma expansion according to the present experiments and as reported in [40, 41, 46] is about 20 km/s. The gap voltage drops along the region that is not occupied yet by the plasma [40, 41, 46]. The expanding plasma maintains a quasi-neutral state, with the potential drop inside it being small, with a negatively charged layer of excessive electron density screening the field on the boundary (see figure 8 of ref. [40, 41, 46]). The fast plasma expansion is driven by the electrostatic force exerted by the residual field on that charged layer, with the ions being "dragged" by its electrons. When this plasma boundary reaches the anode, the entire gap will be filled with the quasi-neutral, highly conductive plasma, which forms a conductive channel causing the collapse of the gap voltage.

Light emission from the expanding plasma can be observed only if the interaction probability between the plasma electrons and ionized or neutrals atoms is high which requires a sufficient plasma density. During the free plasma expansion, the densities in the gap are quite low compared to that in the vicinity of the cathode [41], thus no detectable light is emitted far away from the cathode spot. This changes when the plasma expansion wave front reaches the anode and stops expanding freely. When this happens, the ions both reflect from the anode and sputter the anode material (anode material appears in the anode glow spectra [35]). This increases the total ion and neutral densities in the vicinity of the anode and consequently causes the emission of detectable light due to higher collision rate. This increased density region expands towards the cathode, gradually equilibrating the density all over the gap. Thus, the time when the gap is bridged by light, appears significantly later and is not directly related to the voltage collapse. Finally, after the breakdown enters the steady arc stage, this light gradually decays (see Figure 5). This implies that the final equilibrium plasma density distribution is quite low farther away from the cathode spot, although more investigation is required to explain this phenomenon, which is out of the scope of this work.

5. Conclusions

We experimentally investigated the effect of the anode material on the evolution of vacuum breakdowns by analyzing the dynamics of the light emission from the gap, as recorded by a streak camera, combined with the corresponding current-voltage waveforms. We found that the

choice of anode material does not affect significantly neither the time of appearance of the anodic glow, nor the formation of the conductive channel (voltage collapse). The occurrence of these two events exhibited a very strong temporal correlation; yet, no direct dependence on each another was found, since they appeared in random order, implying that a fully conductive channel can be established without any light emission from the anode. Our findings are consistent with the fast expansion of the cathode plasma, which causes both the voltage collapse and the anode glow when it reaches the anode and densifies by sputtering and reflection. On the other hand, our results are incompatible with the heating and evaporation of the anode by electron bombardment as an explanatory mechanism for the anode glow.

Acknowledgments

This work was supported by the National Natural Science Foundation of China under Project No. 51937009 and No. 51807147, Natural Science Basic Research Plan in Shaanxi Province of China (Program No.2019JM-158). A.K. and F.D. acknowledge support from the CERN K-contract (No. 47207461).

References

[1] B. Jüttner, "Cathode spots of electric arcs," *Journal of Physics D: Applied Physics,* vol. 34, no. 17, p. R103, 2001.

[2] G. McCracken, "A review of the experimental evidence for arcing and sputtering in tokamaks," *Journal of Nuclear Materials,* vol. 93, pp. 3-16, 1980.

[3] J. De Lara *et al.*, "Multipactor prediction for on-board spacecraft RF equipment with the MEST software tool," *IEEE Transactions on Plasma Science,* vol. 34, no. 2, pp. 476-484, 2006.

[4] N. Rozario, H. F. Lenzing, K. F. Reardon, M. S. Zarro, and C. G. Baran, "Investigation of Telstar 4 spacecraft Ku-band and C-band antenna components for multipactor breakdown," *IEEE transactions on microwave theory and techniques,* vol. 42, no. 4, pp. 558-564, 1994.

[5] P. G. Slade, *The vacuum interrupter: theory, design, and application*. CRC press, 2007.

[6] S. Dobert *et al.*, "High gradient performance of NLC/GLC X-band accelerating structures," in *Particle Accelerator Conference, 2005. PAC 2005. Proceedings of the*, 2005, pp. 372-374: IEEE.

[7] A. Descoeudres, Y. Levinsen, S. Calatroni, M. Taborelli, and W. Wuensch, "Investigation of the dc vacuum breakdown mechanism," *Physical Review Special Topics - Accelerators and Beams,* vol. 12, no. 9, p. 092001, 2009.

[8] M. Aicheler *et al.*, "A Multi-TeV linear collider based on CLIC technology: CLIC Conceptual Design Report," SLAC National Accelerator Lab., Menlo Park, CA (United States)2014.

[9] D. Lyon and A. Hubler, "Gap size dependence of the dielectric strength in nano vacuum gaps," *IEEE Transactions on Dielectrics and Electrical Insulation,* vol. 20, no. 4, pp. 1467-1471, 2013.

[10] S. Ducharme, "An inside-out approach to storing electrostatic energy," *ACS Nano,* vol.

3, no. 9, pp. 2447-50, Sep 22 2009.

[11] R. Sterling, M. Hughes, C. Mellor, and W. Hensinger, "Increased surface flashover voltage in microfabricated devices," *Applied Physics Letters,* vol. 103, no. 14, p. 143504, 2013.

[12] G. A. Mesyats, "Ecton mechanism of the cathode spot phenomena in a vacuum arc," *IEEE Transactions on Plasma Science,* vol. 41, no. 4, pp. 676-694, 2013.

[13] G. A. Mesyats, "Ecton or electron avalanche from metal," *Physics-Uspekhi,* vol. 38, no. 6, pp. 567-590, 1995.

[14] A. Kyritsakis, M. Veske, K. Eimre, V. Zadin, and F. Djurabekova, "Thermal runaway of metal nano-tips during intense electron emission," *Journal of Physics D: Applied Physics,* vol. 51, no. 22, p. 225203, 2018.

[15] H. Timko *et al.*, "A One-Dimensional Particle-in-Cell Model of Plasma Build-Up in Vacuum Arcs," *Contributions to Plasma Physics,* vol. 51, no. 1, pp. 5-21, 2011.

[16] H. Timko *et al.*, "From Field Emission to Vacuum Arc Ignition: A New Tool for Simulating Copper Vacuum Arcs," *Contributions to Plasma Physics,* vol. 55, no. 4, pp. 299-314, 2015.

[17] H. Yanagisawa *et al.*, "Laser-induced asymmetric faceting and growth of a nano-protrusion on a tungsten tip," *APL Photonics,* vol. 1, no. 9, p. 091305, 2016.

[18] S. Fujita and H. Shimoyama, "Mechanism of surface-tension reduction by electric-field application: Shape changes in single-crystal field emitters under thermal-field treatment," *Physical Review B,* vol. 75, no. 23, p. 235431, 2007.

[19] G. Fursey, "Field emission in vacuum micro-electronics," *Applied Surface Science,* vol. 215, no. 1-4, pp. 113-134, 2003.

[20] W. P. Dyke and J. K. Trolan, "Field Emission - Large Current Densities, Space Charge, and the Vacuum Arc," (in English), *Physical Review,* vol. 89, no. 4, pp. 799-808, 1953.

[21] W. P. Dyke, J. K. Trolan, E. E. Martin, and J. P. Barbour, "The Field Emission Initiated Vacuum Arc .I. Experiments on Arc Initiation," (in English), *Physical Review,* vol. 91, no. 5, pp. 1043-1054, 1953.

[22] F. Charbonnier, R. Strayer, L. Swanson, and E. Martin, "Nottingham effect in field and t− f emission: Heating and cooling domains, and inversion temperature," *Physical Review Letters,* vol. 13, no. 13, p. 397, 1964.

[23] B. Mazurek and J. D. Cross, "Fast cathode processes in vacuum discharge development," *Journal of Applied Physics,* vol. 63, no. 10, pp. 4899-4904, 1988.

[24] B. Mazurek, A. Nowak, and A. Tyman, "X-ray emission accompanying cathode microdischarge," *IEEE Transactions on Electrical Insulation,* vol. 28, no. 4, pp. 488-493, 1993.

[25] Y. Inada, T. Kamiya, S. Matsuoka, A. Kumada, H. Ikeda, and K. Hidaka, "Two-dimensional electron density visualization over plasma flare in vacuum breakdown process," *Journal of Applied Physics,* vol. 124, no. 8, p. 083301, 2018.

[26] Z. Zhou, A. Kyritsakis, Z. Wang, Y. Li, Y. Geng, and F. Djurabekova, "Direct observation of vacuum arc evolution with nanosecond resolution," *Scientific Reports,* vol. 9, no. 1, p. 7814, 2019/05/24 2019.

[27] G. A. Mesyats and D. I. Proskurovsky, *Pulsed Electrical Discharge in Vacuum* (Springer Series on Atomic, Optical, and Plasma Physics). Berlin: Springer-Verlag

Berlin Heidelberg, 1989.
[28] A. Anders, *Cathodic arcs: from fractal spots to energetic condensation*. Springer Science & Business Media, 2009.
[29] N. C. Shipman, "Experimental study of DC vacuum breakdown and application to high-gradient accelerating structures for CLIC," The University of Manchester, 2014.
[30] Y. Yen, D. Tuma, and D. Davies, "Emission of electrode vapor resonance radiation at the onset of impulsive breakdown in vacuum," *Journal of applied physics,* vol. 55, no. 9, pp. 3301-3307, 1984.
[31] I. Chalmers and B. Phukan, "Breakdown time lags in short vacuum gaps," *Vacuum,* vol. 32, no. 3, pp. 145-150, 1982.
[32] I. D. Chalmers and B. D. Phukan, "Photographic observations of impulse breakdown in short vacuum gaps," (in English), *Journal of Physics D: Applied Physics,* vol. 12, no. 8, pp. 1285-1292, 1979.
[33] G. Mesyats, *Cathode Phenomena in a Vacuum Discharge: The breakdown, the spark, and the arc*. Moscow, Russia: Nauka, 2000.
[34] M. Berger, J. Coursey, M. Zucker, and J. Chang, "Stopping-power and range tables for electrons, protons, and helium ions (2005)," *Available on http://physics.nist.gov/Star,* 2015.
[35] Z. Zhou, A. Kyritsakis, Z. Wang, Y. Li, Y. Geng, and F. Djurabekova, "Spectroscopic study of vacuum arc plasma expansion," *Journal of Physics D: Applied Physics,* vol. 53, no. 12, p. 125501, 2020/01/09 2020.
[36] A. Anders, "The evolution of ion charge states in cathodic vacuum arc plasmas: a review," *Plasma Sources Science and Technology,* vol. 21, no. 3, p. 035014, 2012.
[37] P. A. Ni and A. Anders, "Supersonic metal plasma impact on a surface: An optical investigation of the pre-surface region," *Journal of Physics D: Applied Physics,* vol. 43, no. 13, p. 135201, 2010.
[38] A. Anders and G. Y. Yushkov, "Ion flux from vacuum arc cathode spots in the absence and presence of a magnetic field," *Journal of Applied Physics,* vol. 91, no. 8, pp. 4824-4832, 2002.
[39] I. Krinberg, "Acceleration of a multicomponent plasma in the cathode region of a vacuum arc," *Technical Physics,* vol. 46, no. 11, pp. 1371-1378, 2001.
[40] E. Nefedtsev and A. Batrakov, "Simulations of the Stable Expansion of a Monoelement Three-Component Explosive-Emission Plasma," *Journal of Experimental and Theoretical Physics,* vol. 126, no. 4, pp. 541-549, 2018.
[41] D. L. Shmelev and S. A. Barengolts, "Modeling of cathode plasma flare expansion," *IEEE Transactions on Plasma Science,* vol. 41, no. 8, pp. 1964-1968, 2013.
[42] G. Y. Yushkov, A. S. Bugaev, I. A. Krinberg, and E. M. Oks, "On a mechanism of ion acceleration in vacuum arc-discharge plasma," *Doklady Physics,* journal article vol. 46, no. 5, pp. 307-309, May 01 2001.
[43] J. F. Ziegler. (2013). *SRIM-2003 software package*. Available: http://www.srim.org
[44] A. Anders, S. Anders, A. Forster, and I. G. Brown, "Pressure ionization: its role in metal vapour vacuum arc plasmas and ion sources," *Plasma Sources Science and Technology,* vol. 1, no. 4, p. 263, 1992.
[45] E. Hantzsche, "Consequences of balance equations applied to the diffuse plasma of

vacuum arcs," *IEEE Transactions on Plasma Science,* vol. 17, no. 5, pp. 657-660, 1989.

[46] E. Nefedtsev and A. Batrakov, "Plasma expansion in vacuum gap: Three-fluid hydrodynamic simulation," in *2016 27th International Symposium on Discharges and Electrical Insulation in Vacuum (ISDEIV)*, 2016, vol. 1, pp. 1-4: IEEE.